nature geoscience
SUPPLEMENTARY INFORMATION
DOI: 10.1038/NGEO845

Supplementary Information: Accelerating Uplift in the North Atlantic Region as an Indicator of Ice Loss

Yan Jiang, Timothy H. Dixon, and Shimon Wdowinski

GPS Analysis

We use publicly available data for Greenland and adjacent areas (Figure 1), focusing on data sets that are at least five years in length (most time series are seven years or longer) and contain at least a thousand daily observations (most time series exceed 2,000 data points) (Table S1). We found that acceleration or velocity change estimates for time series shorter than five years are less reliable. To avoid possible systematic errors associated with long term reference frame drift or biases associated with high latitude effects, we compare Greenland data with adjacent northern hemisphere regions, including northeastern Canada and Fennoscandia. The occupation history of GPS sites in Greenland is described in *Khan et al.*[15] We use the GIPSY-OASIS software[31] following techniques described in *Sella et al.*[32], and the IGb00 reference frame[33]. Use of the alternate ITRF 2005 reference frame for vertical motions referenced to the Earth center of mass has been questioned[34]. We computed results in both reference frames. On average, accelerations in ITRF2005 are slightly higher (by about 0.3 mm/yr^2) and have slightly higher RMS misfits. We report results in the IGb00 frame, but note that the basic conclusion of our paper is the same in either frame: accelerations in the vertical component are systematically higher for GPS sites in Greenland, Iceland and Svalbard compared to adjacent north Atlantic regions lacking multiyear land ice. Note that for stable North America and Fennoscandia, mean vertical acceleration in IGb00 is

 DOI: 10.1038/NGEO845

essentially zero (Figure 3). In contrast, results for these areas in ITRF2005 show a positive acceleration of 0.3 mm/yr^2, which we feel is physically implausible.

Time Series Analysis

The least squares models fit to the GPS data have 6-11 parameters, including annual and semi-annual variations (each with a phase and amplitude, for a total of four parameters), and, in the case of equipment changes, one or more offset parameters (maximum three). In addition to these parameters, we fit either a constant velocity model (two additional parameters), a constant acceleration model (three additional parameters, describing initial velocity plus a constant acceleration term) or a "kink" model, with two velocities separated by a "ramp time" (time of instantaneous acceleration, t^*) (four additional parameters). Standard F-test criteria are used to define the appropriate model.

The site position $y(t)$ for a constant velocity model can be written as:

$$y(t_i) = a + bt_i + c\sin(2\pi t_i) + d\cos(2\pi t_i) + e\sin(4\pi t_i) + f\cos(4\pi t_i) + \ldots$$

$$+ \sum_{j=1}^{n_g} g_j H(t_i - T_{gj}) + v_i \qquad \text{(S1)}$$

where t_i, i=0,1,2,3……N are the daily position solutions, a is the site initial position, b is the site linear velocity, and coefficients c,d and e,f describe the annual and semi-annual motion, respectively. The summation term is the correction for any number (n_g) of offsets, with magnitude g and epoch time T. The last term is the measurement error, v.

To extract the acceleration information in a time series, we add an acceleration term kt_i^2 to the above mentioned equation (S1). The parameter k describes the acceleration in a given component for each station.

$$y(t_i) = a + bt_i + kt_i^2 + c\sin(2\pi t_i) + d\cos(2\pi t_i) + \ldots$$

$$+e\sin(4\pi t_i)+f\cos(4\pi t_i)+\sum_{j=1}^{n_g} g_j H(t_i - T_{gj})+v_i \qquad \text{(S2)}$$

We also estimate two linear velocities separated by a "ramp" time, t^* for the 'kink' model. In this case we replace the linear term in equation (S1) by two terms, $b_1 t_i H(t^*-t_i)$ and $b_2 t_i H(t_i-t^*)$, where b_1 and b_2 are the first and second phase of site linear motion velocity, and H is the stepping function that separates the estimates before and after ramp time t^*.

$$y(t_i)=a+b_1 t_i H(t^*-t_i)+b_2 t_i H(t_i-t^*)+c\sin(2\pi t_i)+d\cos(2\pi t_i)+\ldots$$

$$+e\sin(4\pi t_i)+f\cos(4\pi t_i)+\sum_{j=1}^{n_g} g_j H(t_i - T_{gj})+v_i \qquad \text{(S3)}$$

We use a grid search algorithm to estimate t^*. When t^* is specified, the other parameters can be estimated using a linear least-square inversion weighted by the variance of the GPS coordinate estimates. We do the one-dimensional grid search over the entire time t with grid spacing of 0.01 year. At each node, we perform a weighted least square inversion to estimate the model parameters. If the misfit RMS is smaller than the current RMS_{min}, we update t^* to the current ramp time t'. The ramp time uncertainties are estimated at the 95% confidence interval.

Error Analysis

If measurement errors v are independent, normally distributed and random, they can be readily determined during the least square estimation process. Such estimates are often optimistic, but may be scaled upward if independent information is available, e.g., the dispersion of results in terrain thought to be non-accelerating (Figure 3). In reality, the errors are often non-random, associated with different site characteristics and/or equipment used in different time periods. Furthermore, site specific errors such as

 DOI: 10.1038/NGEO845

multipath effects, antenna phase center variations, monument stability and atmospheric noise will reduce GPS precision in complex ways. A simple white noise-only error model may therefore be inadequate[35]. Two error estimation methods are used in our study to estimate model parameter uncertainties. First we use an empirical constant to scale the white noise uncertainties. Second, we use a bootstrap method to estimate uncertainty in the acceleration term[36]. For each station, we randomly select a subset of data points from the observation data pool, estimating an acceleration term for each subset and repeat for 1000 times. The resulting spread of acceleration estimates defines the 95% and 99% confidence interval (Figure S1). Among the Greenland stations we tested, uncertainties range from 0.1 mm/yr^2 to 0.6 mm/yr^2, similar to the scaled white noise estimates. The uncertainty values reported in Table S1 are the larger of the two estimates. The uncertainty show in Figure 4 for the GPS data is the uncertainty in the initial velocity, V_0 (Table S1) or ±0.5mm/yr, whichever is larger.

Results

The time series are shown in Figures S2 (Greenland, Iceland, Svalbard sites) and S3 (remaining sites in Canada, UK and Fennoscandia). In these figures, each data point represents one day of GPS observation (usually a 12-24 hour average). Table S1 shows the time span of the data, the number of data points (N), and key results of the constant acceleration model, including the RMS misfit of the model to the vertical position data, the amplitude of the annual term, the initial velocity, the annual phase minimum, and the acceleration. RMS misfits are 5-10 mm (mean 6.7 mm), about the level expected based on data noise. One station (out of a total of 31) with very high misfit was excluded from further analysis.

Annual variation in the time series reflects annual changes in ice loading, as well as orbital and atmospheric effects[37]. The amplitude of the annual term in our time series ranges from 1-6 mm, and tends to be higher in Greenland, Iceland and Svalbard (mean 3.7 mm) compared to other sites (mean 2.1 mm), presumably reflecting the influence of the changes in surface loading by ice and corresponding elastic response[38]. All of the Greenland, Iceland and Svalbard stations have their annual phase minimum in May or early June (DOY 137-169) except station THU1 (Figure S5), whose antenna is located on a building and may experience additional thermal expansion/contraction of the building and multipath effects. Stations outside of Greenland, Iceland and Svalbard have their annual minimum and maximum randomly distributed in time (Figure S5). The minimum annual phase of the GPS sites corresponds to the annual mass maximum as measured by gravity experiments. Our data also suggest an annual phase maximum at January to early December, which does not agree with the gravity measurement indicating minimum mass loading in September. This may reflect the speed of summer melting, and a delayed crustal response. Both cases require further modeling of the melting and uplift process.

For most Greenland, Iceland and Svalbard time series, constant acceleration models (Figure S2), are a significant improvement compared to constant velocity models. For remaining sites, constant acceleration models are not significantly different from constant velocity models, i.e., accelerations are close to zero, and a simple linear fit (constant velocity) is the appropriate model. For comparison purposes we have nevertheless compiled the acceleration values for all sites (Figures S2 and S3; Tables S1 and S2).

 DOI: 10.1038/NGEO845

Table S2 and Figure S4 compares the constant acceleration model with the kink (two velocity) model for sites in Greenland, Iceland and Svalbard, all of which are experiencing increasing uplift. For Greenland, four of the time series (KELY,THU2, THU3 and the composite time series THUZ) are actually better fit with the simpler, constant acceleration model compared with the kink model. One site, KULU, in southeast Greenland, experiences a large reduction in misfit with the kink model (significant at better than 99%). Two of the sites (THU1 and QAQ1) experience a slight improvement in misfit with the kink model. For Greenland, Iceland and Svalbard sites where the kink model is preferred, the velocity after t* is always higher than the velocity prior to t*.

For the constant acceleration model, velocities at any time are readily computed from the initial velocity and the acceleration. Velocities at times sampled by the data are believed to be accurate to better than ±1 mm/yr (e.g., compare the independent estimates for Thule in 2001 (Figure 4). However, velocity extrapolations beyond the time span sampled by the data become progressively less accurate as extrapolation time increases, representing the combined effects of data noise and the limitations of a constant acceleration model.

Since half the Greenland sites are actually better fit with the constant acceleration model compared to the kink model, we suggest that this simple model adequately approximates the current phase of uplift, and focus on this model for most of our discussion. More sophisticated models for the time variable uplift of Greenland, Iceland and Svalbard (e.g., variable acceleration or multiple velocity models) will eventually be required as additional data are acquired and the influence of multiple processes can be better discerned, but for the most part do not appear to be warranted at the present time.

From a physical standpoint, it is unlikely that acceleration at the high rates we infer could continue for more than a few additional decades.

Additional Information on Figure 4

Figure 4 compares several of estimates of Greenland mass balance, published in 2005 and later, for comparison to the GPS estimates of uplift. Note that the GPS uplift data are essentially a mirror image of the mass balance data, implying that uplift is an essentially instantaneous effect of significant ice melting. Additional sources of information compiled in this figure include: *Velicogna and Wahr*[39], *Ramillien et al.*[40] *and Chen et al.*[41]

Comparison of the GPS data to GIA models for the vertical motion at sites in western Greenland that began recording in 1995 (KELY plus Thule sites) suggests that acceleration began in the late 1990's, which is consistent with both the retreat of the glacier margins at this time,[42,43] as well as the general warming observed in intermediate depth waters in the Labrador Sea and Davis Straight.[44,45] Taking into account the velocity uncertainties, and assuming 1mm/yr uncertainty in the GIA model, suggests that accelerated uplift of the Thule and KELY GPS sites depart from GIA-predicted values by no later than 1999-2000 (best estimate 1998). Air temperatures in western Greenland at this time were apparently stable[44], implying that increased melting at the edge of glaciers terminating in the ocean, rather than increased surface melting, was the major cause of accelerating uplift.

DOI: 10.1038/NGEO845

References

31. Zumberge, J. F., Heflin, M. B., Jefferson, D. C., Watkins, M. M., and Webb, F. H., Precise point positioning for the efficient and robust analysis of GPS data from large networks, *J. Geophys. Res.* **102**(B3), 5005-5017 (1997).

32. Sella, G. F., Dixon, T. H., & Mao, A., REVEL: A model for Recent plate velocities from space geodesy *J. Geophys. Res.* **107**, B4, 10.1029/2000JB000033 (2002).

33. Ray, J., Dong, D., & Altamimi, Z., IGS reference frames, *GPS Solutions* **8,** 251-266 (2004).

34. Argus, D., Defining the translational velocity of the reference frame of Earth, *Geophys. J. Int.* **169,** 830–838 doi: 10.1111/j.1365-246X.2007.03344.x (2007).

35. Mao, A., Harrison, C. G. A., & Dixon, T. H., Noise in GPS coordinate time series, *J. Geophys. Res.*, 104(B2), 2797–2816, (1999).

36. Press, W. H., Teukolsky, S. A., Vetterling, W. T. & Flannery, B. P., Numerical Recipes in FORTRAN, 2nd Edition, Cambridge (1992).

37. Dong, D., Fang, P., Bock, Y., Cheng, M. K., and Miyazaki, S., Anatomy of apparent seasonal variations from GPS-derived site position time series, *J. Geophys. Res.*, 107(B4), 2075-2092, doi:10.1029/2001JB000573, (2002).

38. Farrell, W. E., Deformation of the Earth by surface loads, Rev. Geophys. Space

Phys., 10, 761-797 (1972).

39. Velicogna, I., & Wahr, J., Acceleration of Greenland ice mass loss in spring 2004, Nature 443, 329– 331, doi:10.1038/nature05168 (2006).

40. Ramillien, G. et al., Interannual variations of the mass balance of the Antactica and Greenland ice sheets from GRACE, Global Planetary Change 53, 198-208 (2006).

41. Chen, J. L., Wilson, C. R., & Tapley, B. D., Satellite gravity measurements confirm accelerated melting of Greenland ice sheet, Science 313, 1958-1960, doi:10.1126/science.1129007 (2006).

42. Joughin, I., W. Abdalati, M. Fahnestock Large fluctuations in speed on Greenland's Jakobshavn glacier. Nature 432, 608-610, doi:10.1038/nature 03130 (2004).

43. Luckman, A., & Murray, T., Seasonal variation in velocity before retreat of Jakobshavn Isbræ, Greenland, *Geophys. Res. Lett.*, 32, L08501, doi:10.1029/2005GL022519 (2005).

44. Holland, D. M., Thomas, R. H., Young, B., Ribergaard, M. H. and Lyberth, B., Acceleration of Jakobshavn Isbræ triggered by warm subsurface ocean waters, Nature Geoscience 1, 659-664, doi:10.1038/ngeo316 (2008).

45. Myers, P. G., Kulan, N. and Ribergaard, M. H., Irminger Water variability in the West Greenland Current, *Geophys. Res. Lett.*, 34, L17601, doi:10.1029/2007GL030419 (2007).

DOI: 10.1038/NGEO845

46. Joughin, I., M. Howat, M. Fahnestock, B. Smith, W. Krabill, R. B. Alley, H. Stern, M. Truffer Continued evolution of Jakobshavn Isbrae following its rapid speedup, J. Geophys. Res., 113, doi:10.1029/2008JF001023 (2008).

Table S1. GPS uplift data fit to a simple model of constant acceleration

Site	Latitude	Longitude	T_{start}	T_{stop}	N	rms	Amp	Min	V_0	Acceleration
	(deg N)	(deg E)	(yr)	(yr)	(Day)	(mm)	(mm)	(DoY)	(mm/yr)	(mm/yr/yr)
Greenland										
KELY	66.99	-50.94	95.56	08.80	2891	7.0	4.4	149	-5.3±0.2	+0.8±0.1
KULU	65.58	-37.15	00.00	08.85	2880	6.6	4.1	143	-0.1±0.6	+1.6±0.2
QAQ1	60.72	-46.05	01.79	08.85	2263	4.9	4.2	165	1.1±0.9	+0.6±0.3
THUZ	76.54	-68.83	95.33	08.85	4478	7.9	3.3	159	-2.6±0.2	+1.1±0.1
THU1	76.54	-68.79	95.33	01.30	1864	9.0	5.5	247	-1.4±1.0	+0.6±0.8
THU2	76.54	-68.83	01.33	08.85	2614	6.5	2.2	137	1.7±0.8	+1.6±0.3
THU3	76.54	-68.83	00.88	08.85	2244	6.0	1.7	137	0.7±1.2	+1.4±0.4
Iceland, Svalbard										
HOFN	64.27	-15.20	97.40	08.85	3990	7.4	5.3	160	4.8±0.4	+1.0±0.1
NYAL	78.93	11.87	94.00	08.85	4893	8.7	2.5	148	4.3±0.2	+0.5±0.1
NYA1	78.93	11.87	98.19	08.85	3756	7.8	1.7	142	7.1±0.5	+0.5±0.2
REYK	64.14	-21.96	96.46	08.85	4334	6.9	4.8	169	-4.6±0.4	+0.6±0.1
REYZ	64.14	-21.96	98.70	07.71	2810	6.6	4.3	168	-2.7±0.5	+0.4±0.2
Canada										
ALRT	82.49	-62.34	02.54	08.85	2165	7.1	4.0	287	8.7±1.7	-0.1±0.6
NAIN	56.54	-61.69	02.96	08.85	2061	5.3	2.0	86	3.7±1.3	+0.4±0.5
RESO	74.69	-94.89	01.69	08.85	2423	7.2	2.0	143	2.8±1.0	+0.9±0.4
SCH2	54.83	-66.83	97.66	08.85	3967	7.1	2.9	94	8.8±0.3	+0.1±0.1
STJO	47.60	-52.68	93.00	08.85	5593	7.2	1.0	28	-1.0±0.2	+0.1±0.1
Fenno-scandia										
BUDP	55.74	12.50	03.00	08.60	2039	4.6	1.5	289	11.0±1.2	-1.0±0.4
JOEN	62.39	30.10	99.16	08.85	3363	6.3	2.1	120	3.7±0.4	0.0±0.2
KIR0	67.88	21.06	99.16	08.85	3505	6.3	3.2	362	6.9±0.4	+0.4±0.2
MAR6	60.60	17.26	99.16	08.85	3506	5.2	2.6	18	7.0±0.3	+0.2±0.1
SPT0	57.71	12.89	01.67	08.85	2606	5.2	0.7	270	3.7±0.7	+0.2±0.3
TROM	69.66	18.94	94.00	08.85	3558	7.5	1.7	126	-1.6±0.4	+0.5±0.1
VAAS	62.96	21.77	99.16	08.85	3331	8.0	2.4	274	8.5±0.5	-0.1±0.2
VARS	70.34	31.03	00.92	08.60	2679	6.5	2.1	320	3.1±0.7	+0.3±0.3
VIL0	64.70	16.56	97.82	08.85	3840	5.6	0.4	302	8.0±0.2	+0.2±0.1
VIS0	57.65	18.37	99.16	08.85	3457	6.3	1.6	27	2.8±0.4	0.0±0.2
Other										
ABEB	57.14	-2.08	98.71	08.24	3258	6.7	2.0	250	4.7±0.4	-0.6±0.2
MORP	55.21	-1.69	96.83	08.85	2978	10.0	4.4	229	-0.9±0.4	+0.2±0.2
NSTG	55.01	-1.44	98.22	08.85	2448	6.3	1.4	261	3.8±1.0	-0.4±0.4
RIGA	56.95	24.06	99.16	08.85	3477	6.5	2.6	31	3.5±0.8	-0.6±0.4

DOI: 10.1038/NGEO845

Notes for Table S1:

$T_{start, stop}$: beginning, end of GPS time series, in years, omitting first two digits (19 or 20).
N: number of days of data in GPS time series.
rms: weighted root mean square misfit of the multi-parameter model to the time series.
Amp: amplitude of annual variation.
V_0: estimated vertical velocity at the beginning of the time series. The reported uncertainties are formal errors (plus or minus one standard deviation) and do not account for systematic biases, e.g. reference frame effects. Computed velocities at other times are believed to be accurate to about ±1 mm/yr within the time span sampled by the data, and progressively less accurate beyond this time span as extrapolation time increases.
Min: Minimum GPS height in the time series, indicating day of year for maximum loading.

Table S2. Comparison of constant acceleration and kink (two-velocity) model for GPS sites in Greenland, Iceland and Svalbard

Site	V_0	V_f	Acceleration	rms		V_1	V_2	*t**	rms
	(mm/yr)	(mm/yr)	(mm/yr/yr)	(mm)		(mm/yr)	(mm/yr)	(yr)	(mm)
Greenland									
KELY	-5.3±0.2	5.3±0.2	+0.8±0.1	7.01		-2.7±0.3	2.9±0.2	2002.0±1.5	7.05
KULU	-0.1±0.6	14.1±0.6	+1.6±0.2	6.60		1.7±0.4	10.6±0.2	2003.5±0.4	6.20
QAQ1	1.1±0.9	5.3±0.9	+0.6±0.3	4.93		3.0±0.3	5.6±0.6	2006.7±2.1	4.91
THUZ	-2.6±0.2	12.3±0.2	+1.1±0.1	7.90		2.0±0.2	9.6±0.3	2003.7±0.9	8.12
THU1	-1.4±1.0	0.6±1.3	+0.6±0.8	9.02		-0.7±0.8	1.8±0.8	1998.4±2.5	9.00
THU2	1.7±0.8	13.7±0.9	+1.6±0.3	6.48		4.1±0.5	9.9±0.3	2004.7±3.6	6.60
THU3	0.7±1.2	11.9±1.3	+1.4±0.4	5.95		7.0±0.3	13.5±1.0	2007.1±1.2	5.96
Iceland, Svalbard									
HOFN	4.8±0.4	16.3±0.4	+1.0±0.1	7.37		6.3±0.3	13.3±0.2	2002.4±0.9	7.15
NYAL	4.3±0.2	11.7±0.2	+0.5±0.1	8.67		6.5±0.2	11.0±0.2	2002.1±1.3	8.51
NYA1	7.1±0.5	12.4±0.5	+0.5±0.2	7.80		6.9±0.4	10.7±0.2	2002.4±1.2	7.54
REYK	-4.6±0.4	2.8±0.4	+0.6±0.1	6.95		-2.4±0.2	1.8±0.2	2003.5±1.3	6.91
REYZ	-2.7±0.5	0.9±0.5	+0.4±0.2	6.58		-1.9±0.4	0.2±0.3	2003.1±3.0	6.56

Notes for Table S2
Symbols are the same as in table 1, except:
V_f is velocity at end of time series in constant acceleration model
V_1 and V_2 are the early and late phase velocities for the kink model
t* is the ramp time in years separating V_1 andV_2.

Table S3. Model parameters and results calculated for the four Greenland stations.

Site	Acceleration	Location	Distance from ice sheet	Additional Line load per year	Uncertainty range
	(mm/yr/yr)		(km)	(N/m/yr/yr)	(N/m/yr/yr)
KULU	+1.6±0.2	East coast	65±5	12.5 x10^7	8.0-20.5 x10^7
QAQ1	+0.6±0.3	South coast	50±5	4.1x10^7	1.5-8.0 x10^7
KELY	+0.8±0.1	West coast	40±5	5.0 x10^7	3.3-8.0 x10^7
THUZ	+1.1±0.1	West coast	15±5	5.2 x10^7	3.5-8.0 x10^7

Model parameters common to all sites are: strip half width (a = 15±5 km), far field reference point (x_{RP} = 400±100 km), and elastic parameters (ν=0.25 and G=30±3 GPa).

DOI: 10.1038/NGEO845

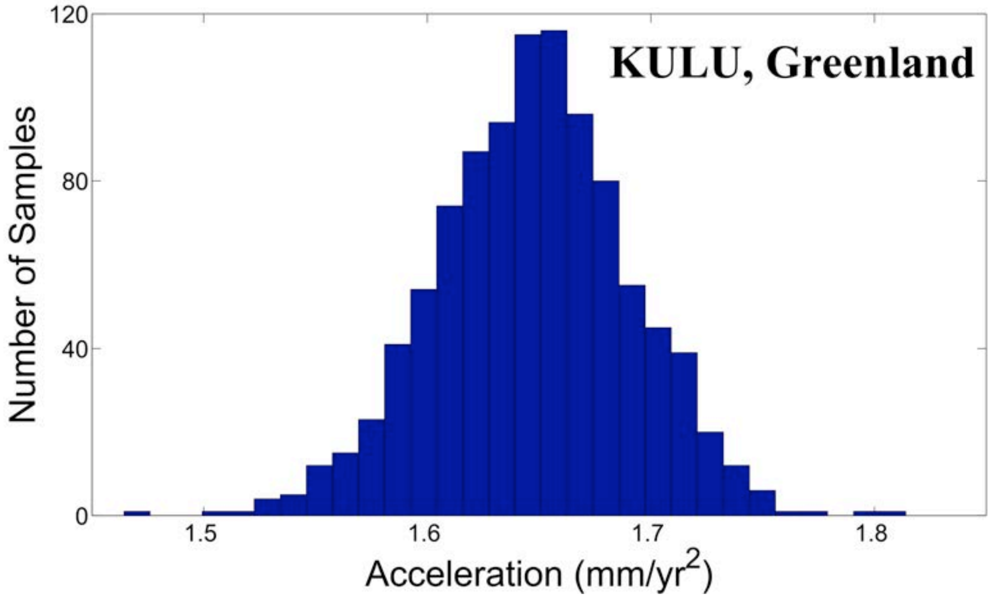

Figure S1. Histogram showing bootstrap result for GPS station KULU in Greenland. Acceleration results are normally distributed, with 99% of the results lying between ±0.15 mm/yr^2 of the best estimate 1.64 mm/yr^2.

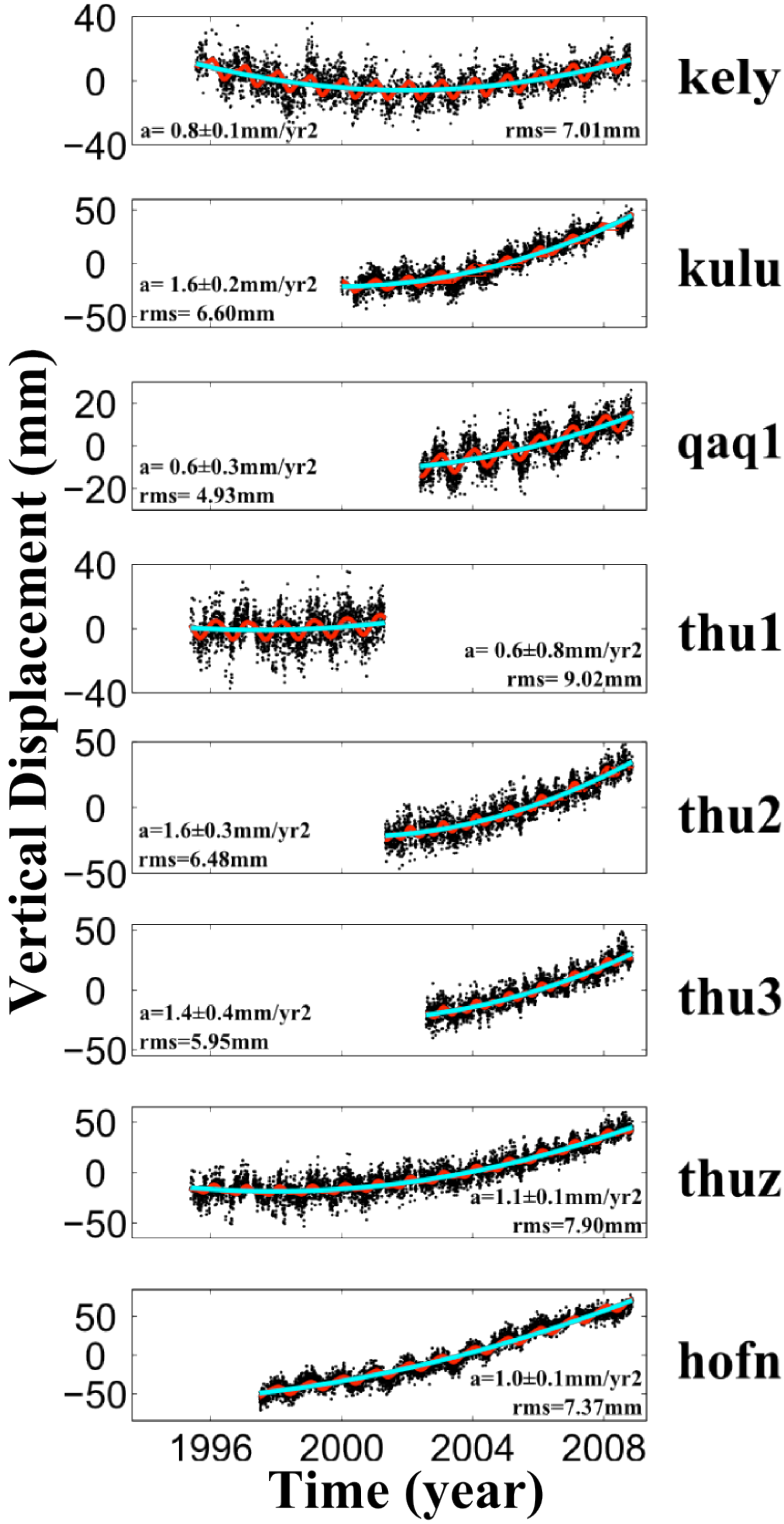
40
0
−40
a= 0.8±0.1mm/yr2
rms= 7.01mm
kely
50
0
−50
a= 1.6±0.2mm/yr2
rms= 6.60mm
kulu
20
0
−20
a= 0.6±0.3mm/yr2
rms= 4.93mm
qaq1
40
0
−40
a= 0.6±0.8mm/yr2
rms= 9.02mm
thu1
50
0
−50
a=1.6±0.3mm/yr2
rms=6.48mm
thu2
50
0
−50
a=1.4±0.4mm/yr2
rms=5.95mm
thu3
50
0
−50
a=1.1±0.1mm/yr2
rms=7.90mm
thuz
50
0
−50
a=1.0±0.1mm/yr2
rms=7.37mm
hofn
Vertical Displacement (mm)
1996
2000
2004
2008
Time (year)

Figure S2a

DOI: 10.1038/NGEO845

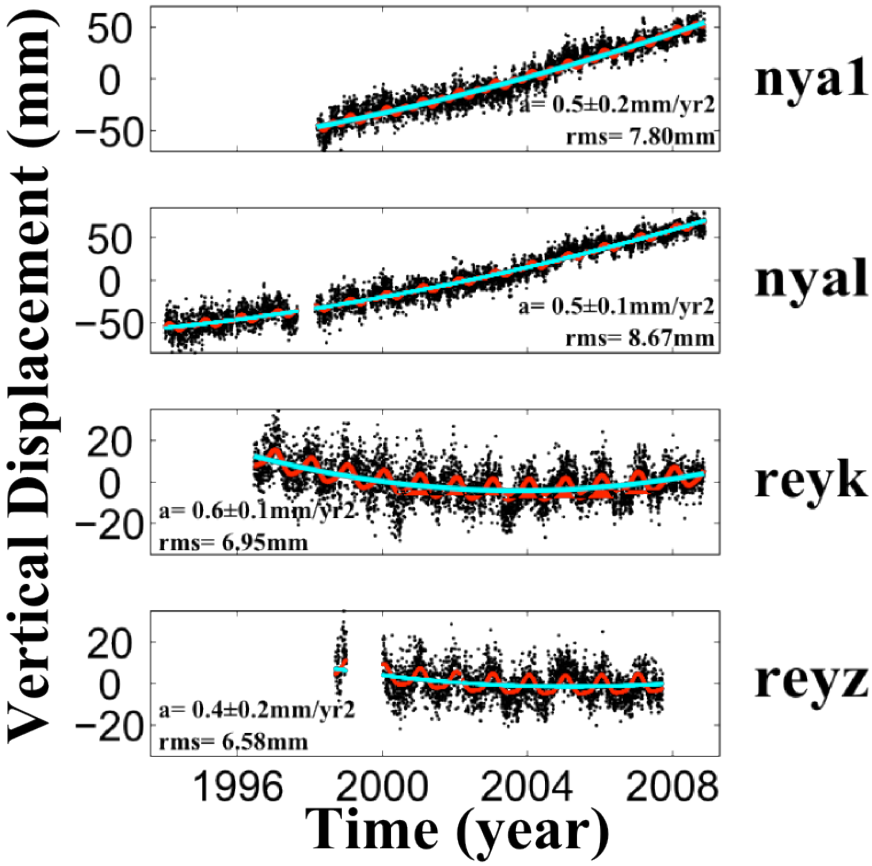

Figure S2. Time series of GPS vertical component position estimates for Greenland, Iceland and Svalbard sites (time in years on horizontal axis, vertical position in mm relative to arbitrary initial position on vertical axis). Red curve shows multi-parameter constant acceleration model, including annual and semi-annual variation; light blue curve shows just the acceleration and initial velocity components of the model. Acceleration (a) and rms misfit are shown in the panel for each time series. Site locations given in Figure 1 (main article) and Table S1.

DOI: 10.1038/NGEO845

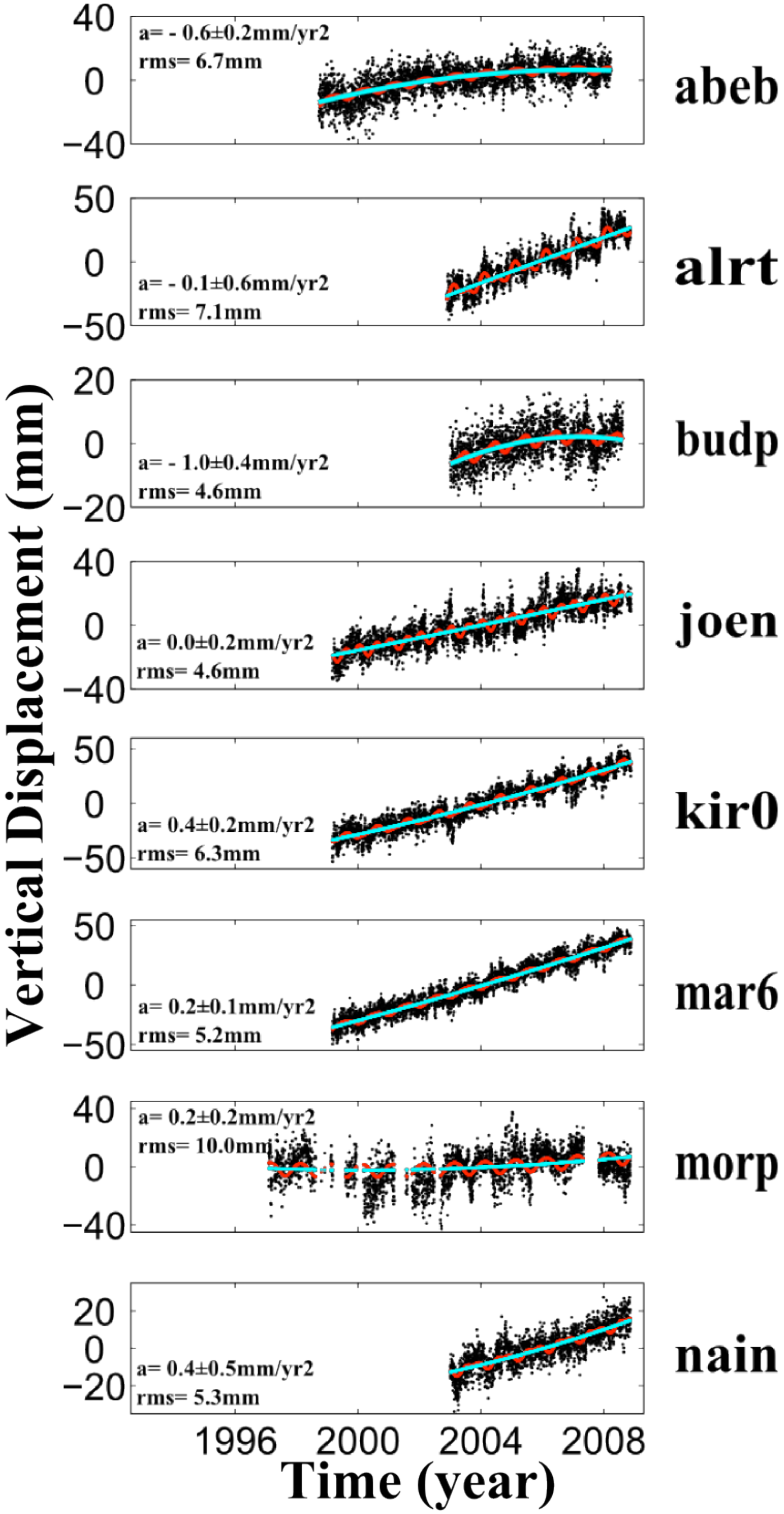

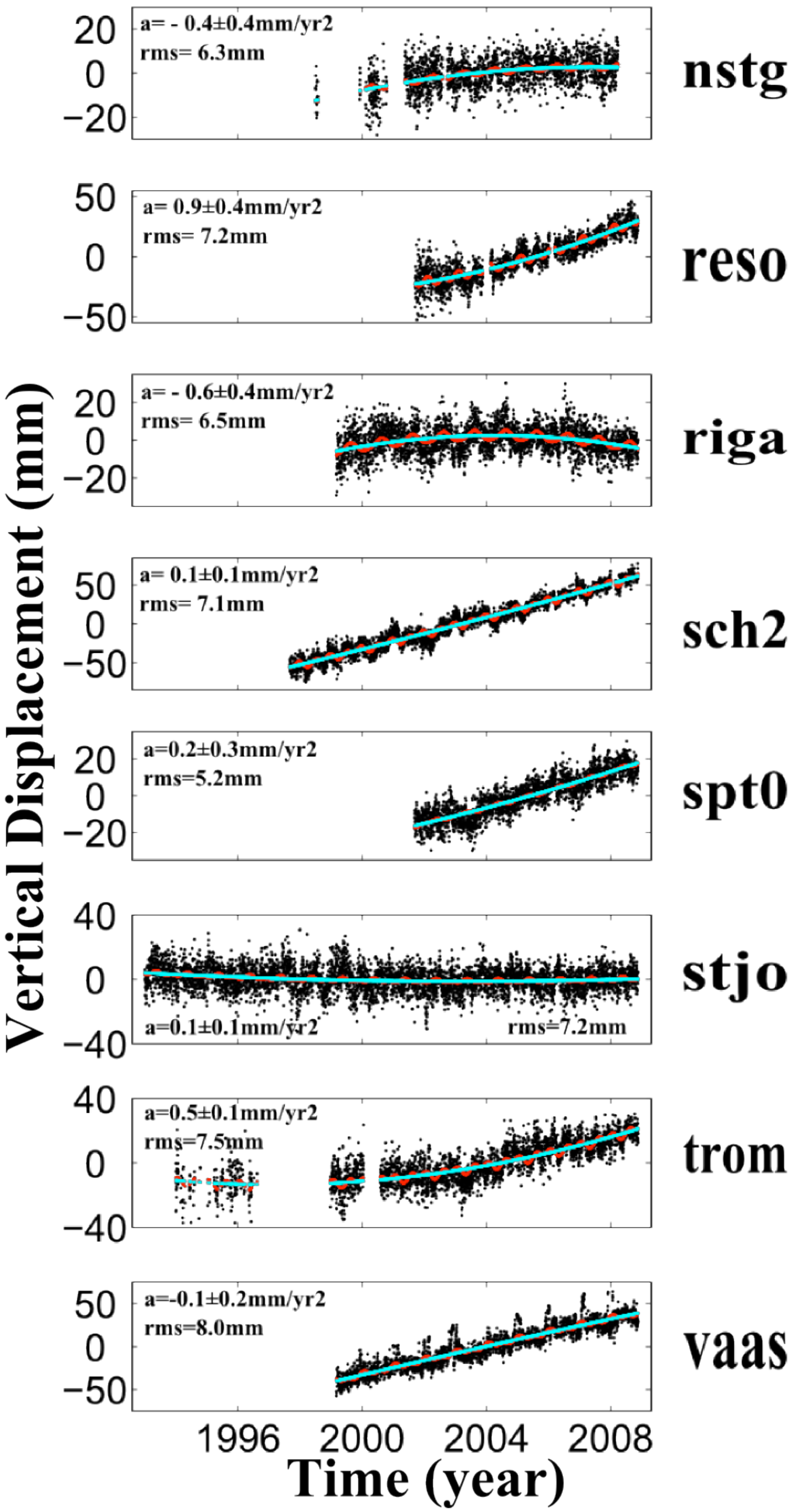
a= - 0.4±0.4mm/yr2
rms= 6.3mm
nstg
a= 0.9±0.4mm/yr2
rms= 7.2mm
reso
a= - 0.6±0.4mm/yr2
rms= 6.5mm
riga
a= 0.1±0.1mm/yr2
rms= 7.1mm
sch2
a=0.2±0.3mm/yr2
rms=5.2mm
spt0
a=0.1±0.1mm/yr2
rms=7.2mm
stjo
a=0.5±0.1mm/yr2
rms=7.5mm
trom
a=-0.1±0.2mm/yr2
rms=8.0mm
vaas
Vertical Displacement (mm)
Time (year)
1996
2000
2004
2008

 DOI: 10.1038/NGEO845

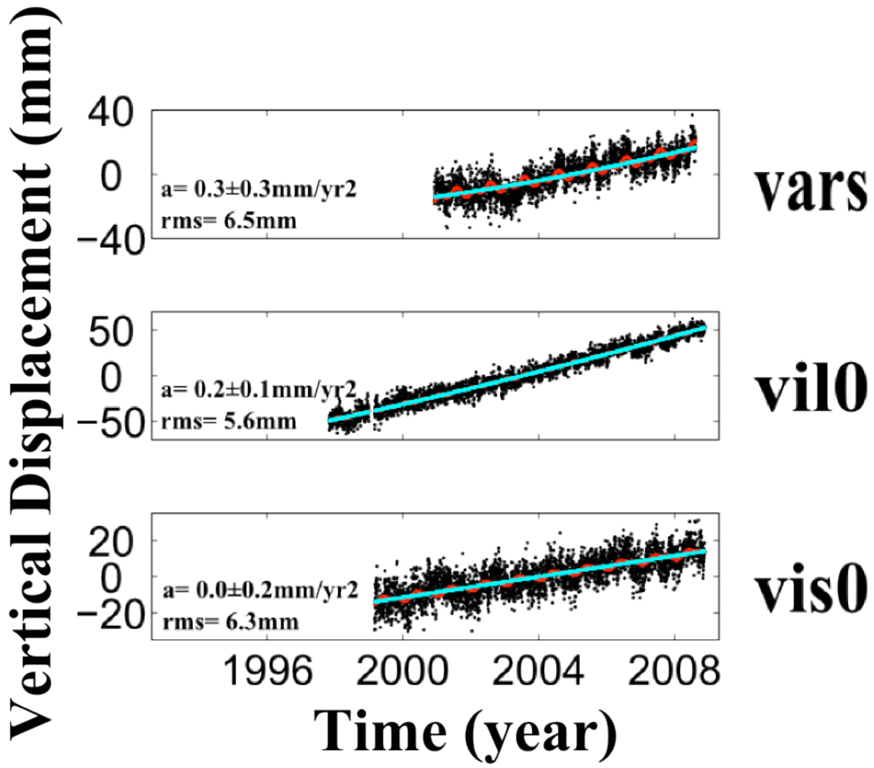

Figure S3. Similar to Figure S2, for sites in Canada, UK and Fennoscandia.

 DOI: 10.1038/NGEO845

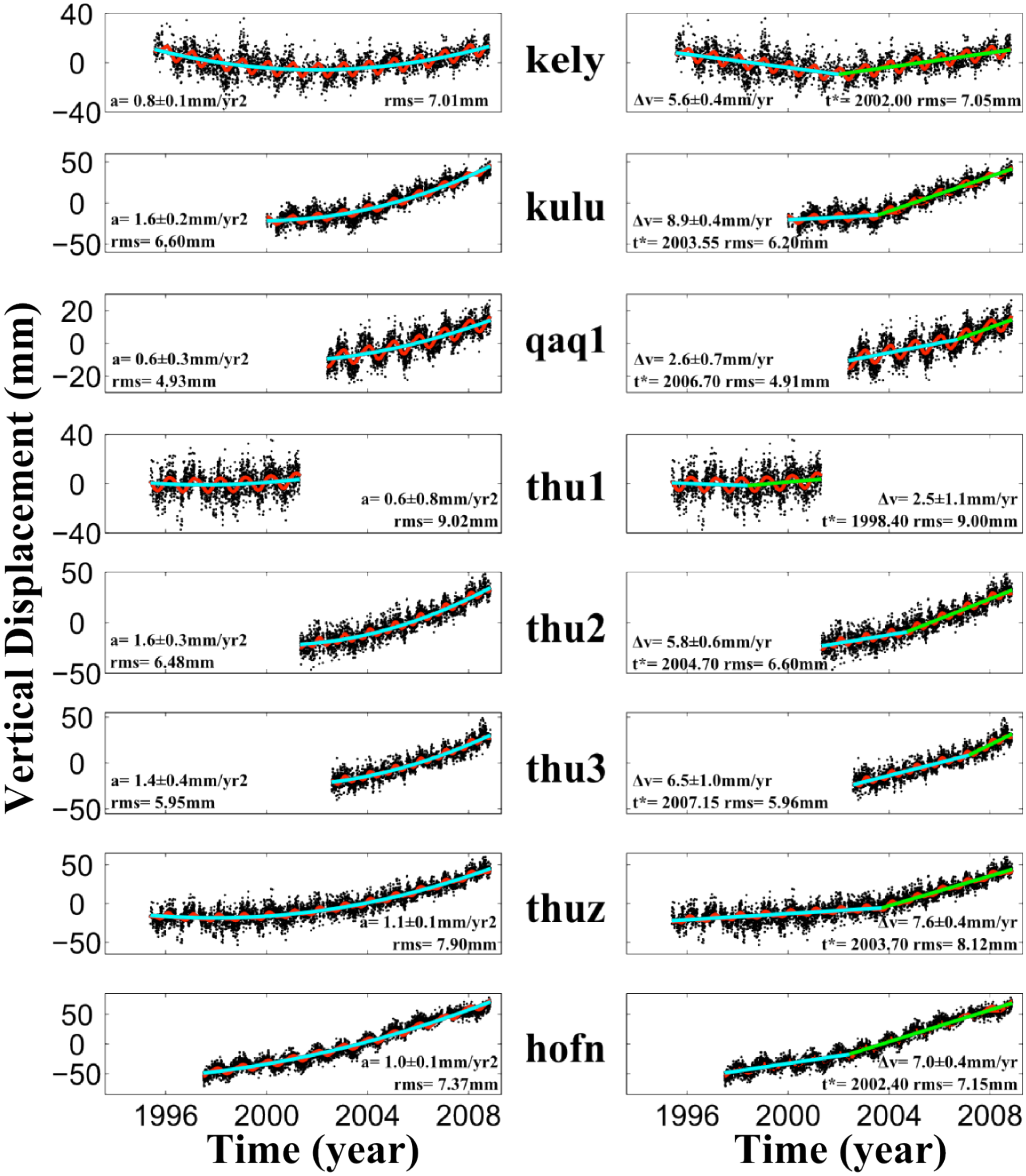

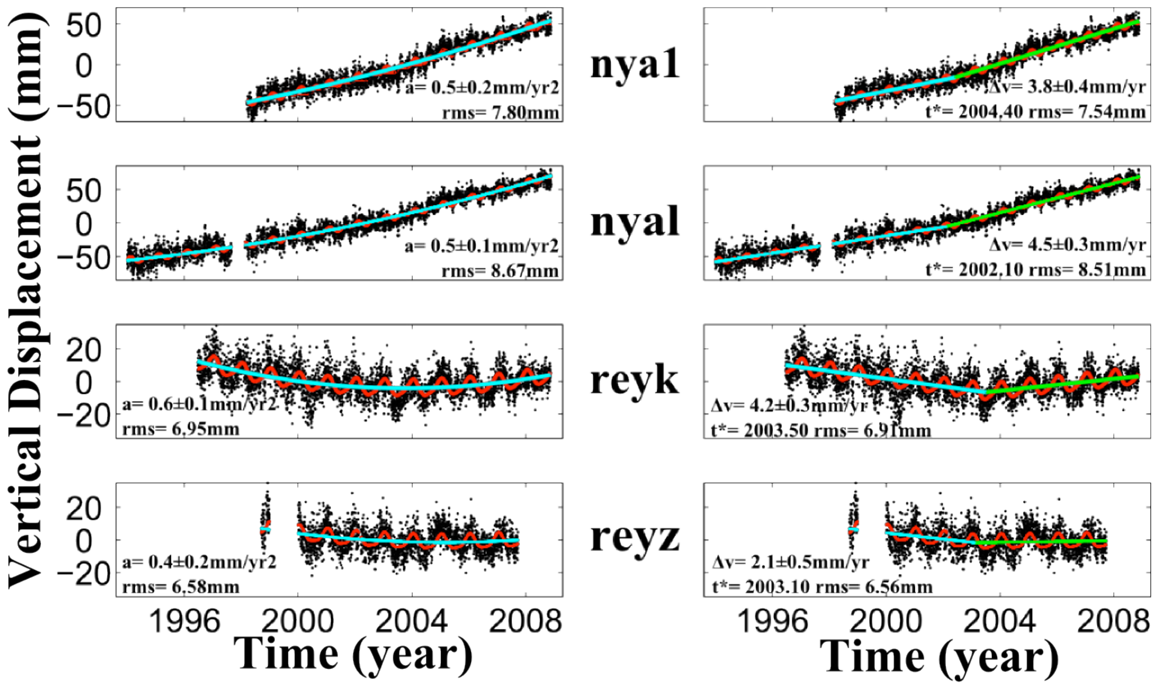

Figure S4. Similar to Figure S2, showing time series for Greenland, Iceland and Svalbard sites, comparing constant acceleration model (left side), and "kink" (two velocity) model (right side). Ramp time ($t*$), velocity change and rms misfit for the kink model are shown in the panel for each time series.

DOI: 10.1038/NGEO845

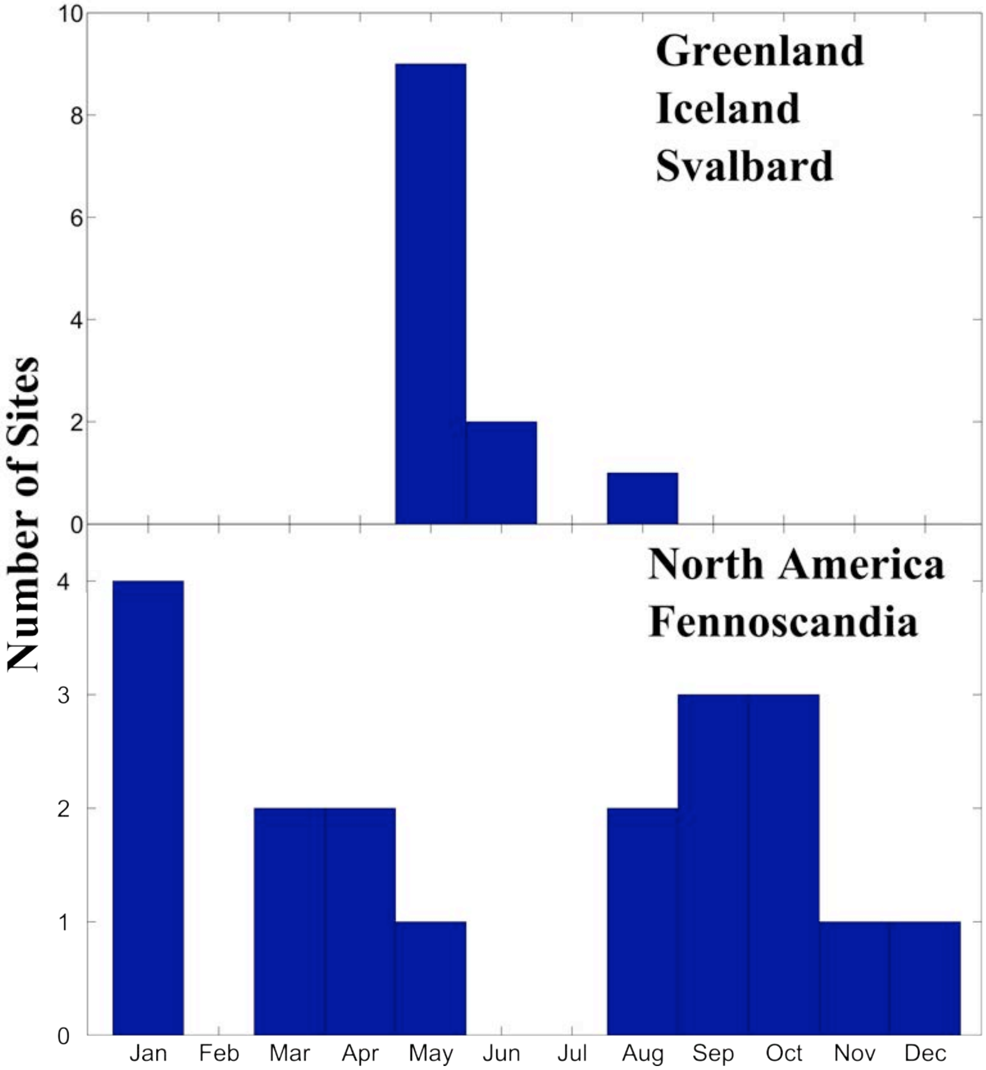

Figure S5 Histogram show the time of minimum surface height for GPS sites.

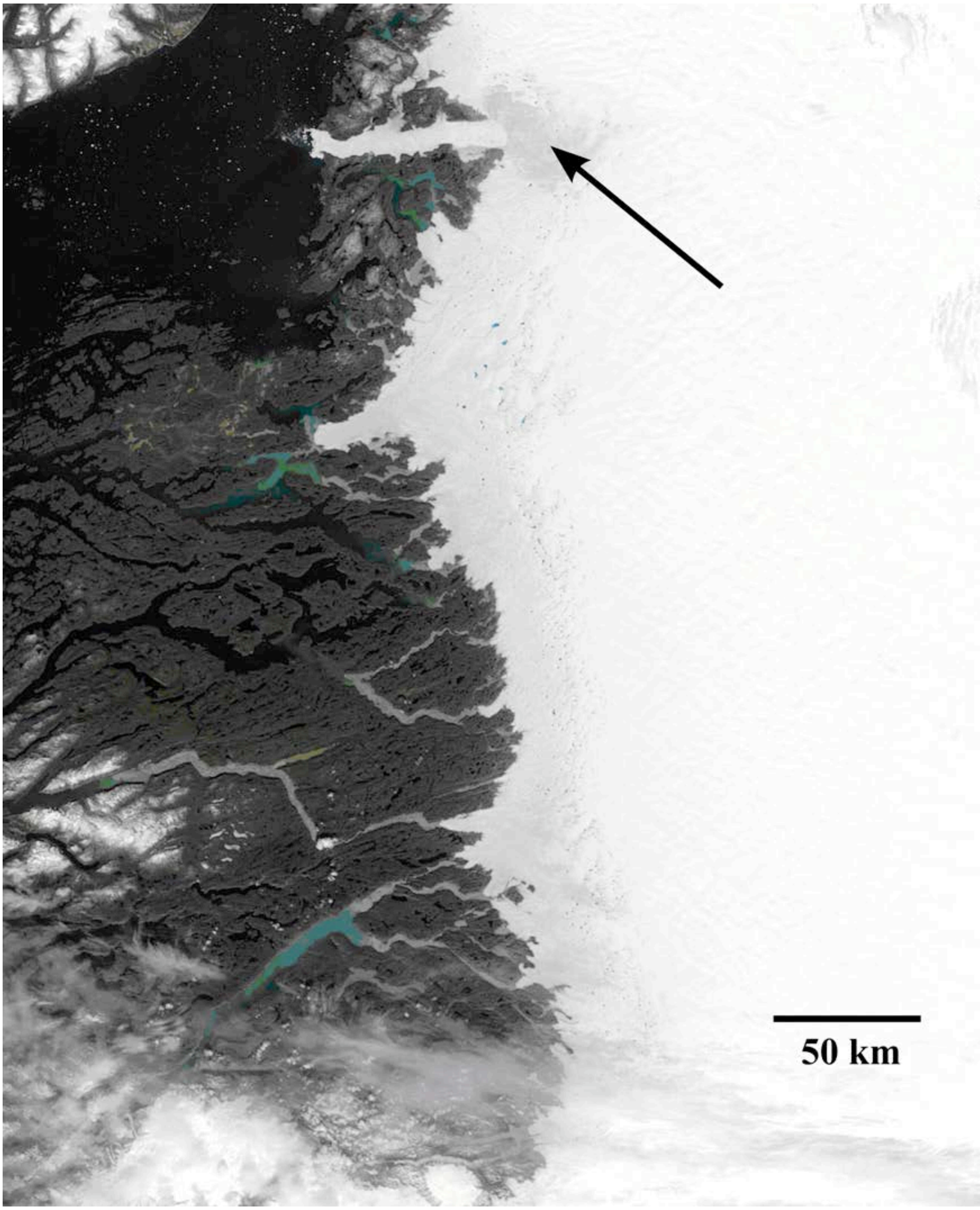

Figure S6. Summer 2006 image of part of Western Greenland, acquired by NASA's MODIS satellite. Note the narrow (~ 30 km wide) band of grey (melting) ice in the center of the image, between the rocky coast to the left (west) and thicker, non-melting, higher altitude ice to the right (east). The narrowness of this band supports the use of a two-dimensional model. The grey ice band includes a number of small lakes which form during the summer melt season. The majority of Greenland's mass loss occurs in such coastal regions, either by melting, or by iceberg calving. Arrow points to darker grey zone of rapidly thinning ice near the outlet of Jacobshavn glacier[42, 46].